ELSEVIER

Journal of Nuclear Materials 256 (1998) 166–179

journal of nuclear materials

Dynamic behavior of hydrogen atoms with a boronized wall

K. Tsuzuki [a,*], N. Inoue [a], A. Sagara [a], N. Noda [a], O. Motojima [a], T. Mochizuki [b], T. Hino [b], T. Yamashina [b]

[a] *Graduate University Advanced Studies, National Institute for Fusion Science, Oroshi-cho 322-6, Toki 509-52, Japan*
[b] *Department of Nuclear Engineering, Hokkaido University, Sapporo 060, Japan*

Received 12 June 1997; accepted 6 April 1998

Abstract

Dynamic behavior of hydrogen atoms in boron films, which is one of candidate materials of the first wall of fusion devices, has been studied. Hydrogen absorption behavior was investigated with a glow discharge in hydrogen. After a strong absorption in the beginning of the discharge, hydrogen atoms were slowly and continuously absorbed for 10 h without saturation. The slow absorption is due to deeper migration of hydrogen atoms into the film, enhanced by the ion bombardment. A helium glow discharge causes both ion induced desorption and the deeper migration, and thus, hydrogen atoms are accumulated in the film when the H_2 and He discharges are repeated alternately. Most of the retained hydrogen atoms were released by heating up to 400°C. A calculation result based on a simple model was compared with the experimental results. A recombination coefficient was obtained from the analysis of the experimental transient release of the H atoms just after the H_2 discharge. The time behavior at the initial phase of the He discharge was reproduced fairly well with use of a smaller cross-section for the He^+ ion induced detrapping than that for H_2^+.

1. Introduction

It is known that plasma-facing first wall in fusion devices plays an important role for impurity and fuel control. Aiming a reduction of metal impurities, and thus, radiation losses, low Z materials like carbon, boron, beryllium, and lithium have been employed in many devices and investigated for many years [1–11].

In situ boron coating (boronization) was first applied in TEXTOR in 1989 [4]. Reduction of carbon and oxygen impurities due to oxygen gettering ability of the boron films was observed compared to the carbonized wall. Improvement in plasma performance has been achieved for most of the devices with the boronization [4–9]. In addition, hydrogen recycling from the boron film is relatively lower compared to the carbon walls [4,5]. Boronization is planned in large helical device (LHD) because of the above noted merits. However, one of the concerns in LHD is hydrogen behavior, especially recycling with a low temperature wall, since the baking temperature is limited less than 100°C [12]. Thus, in this work, we focus our attention to hydrogen behavior in the boron coating films.

Understanding of the hydrogen re-emission is important from a view point of fuel control when low Z materials are used, which retain a large amount of hydrogen atoms. The plasma density control becomes difficult if a considerable number of hydrogen atoms are re-emitted (recycled) from the wall because the density increases without external fueling [13]. In addition, it has been reported that low recycling condition is favorable to obtain good energy confinement [14]. The reduction of hydrogen recycling at a wall surface is an important issue for better density control and performance in the present devices.

For long term discharges, transient release of excess hydrogen atoms may take place under some conditions, which makes plasma density control difficult [15]. Understanding of dynamic behavior of the hydrogen recycling is important for better control. Tritium inventory

* Corresponding author. Tel.: +81-57 258 222; fax: +81-57 258 2618; e-mail: tuzuki@nifs.ac.jp.

0022-3115/98/$19.00
PII: S0022-3115(98)00062-2

will be a serious problem in DT burning devices. Thus, it is important not only to reduce the hydrogen recycling but also to understand hydrogen behavior precisely for future devices.

It has been reported that high temperature baking is effective to reduce the hydrogen recycling. In devices such as JT-60U, TEXTOR, and DIII-D, in which the wall temperature can be heated up to 300°C, the hydrogen recycling is well reduced with the boronized wall compared to the carbonized wall [4–6]. On the other hand, hydrogen recycling is similar to the carbonized wall in devices in which the wall temperature is limited at around room temperature [7–9]. Helium glow discharge is widely applied to boronized or carbonized walls and it has been found to be effective for reduction of the hydrogen recycling [16,17]. Dynamic behavior has been investigated in JET with a carbon and a beryllium wall [18]. However, the basic mechanism of the recycling is not well understood.

In this study, basic data on re-emission from boron films are obtained by hydrogen implantation, helium ion bombardment, and thermal desorption. Measurements with high precision are achieved by using a liner which has a large surface area as described in Section 2. Experimental results are presented in Section 3. In order to understand hydrogen behavior in the boron film, a simple theoretical model is proposed and compared with the experimental results, which is discussed in Section 4.1. A possible application of the boron films to future devices is discussed in Section 4.2.

2. Experimental

An experimental device named SUT (SUrface modification Teststand) was mainly used in this study. Fig. 1 shows a schematic view of the device. The distinctive feature of the device is (1) achievement of ultra high vacuum condition which enables us to prepare clean, impurity-free films, (2) possible replacement of liner with a large surface area of 7000 cm^2, which can be heated up to 600°C, and (3) in situ Auger electron spectroscopy (AES) measurement.

In this chamber, a cylindrical liner used was 400 mm in diameter, 400 mm in height, and 7000 cm^2 in surface area. It is changeable and replaced to new and clean one if necessary. The effect of the liner material could be investigated. So far, the liner made of stainless steel and graphite were used. The results with stainless steel liner are mainly shown in this paper. The liner could be heated up to 600°C by molybdenum heaters installed in the chamber. The boron film was deposited on the whole inner surface of the liner by a DC glow discharge in B_2H_6 (5%) + He (95%). After the coating, the glow discharges in H_2 and He were carried out. Ions generated in the plasma were accelerated to a few hundreds eV and

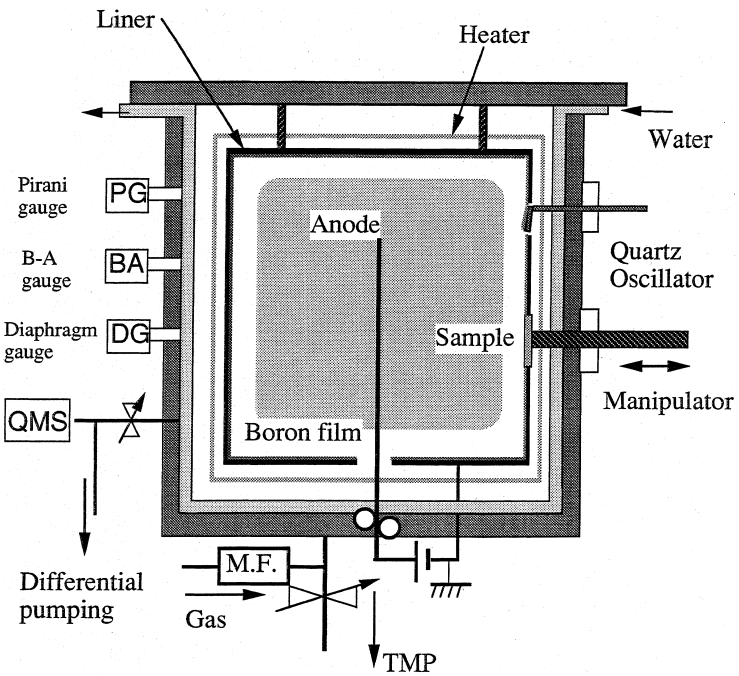

Fig. 1. Cross-sectional view of main chamber of SUT.

implanted to the film. The amount of hydrogen absorption and desorption was obtained from the pressure change measured by a diaphragm gauge (DG) and a quadrupole mass spectrometer (QMS). Thermal desorption measurement was carried out by raising the whole liner temperature up to 500°C. All these procedures were done under an ultra high vacuum condition with a background pressure of 10^{-7} Pa, and thus, the impurity concentration in the boron film was kept less than a few percents, which was confirmed by an in situ AES.

The experimental procedure consists of three stages; namely (1) film preparation, (2) discharge experiments, and (3) thermal desorption. In the stage (1), boron films were deposited by the discharge in B_2H_6(5%) + He(95%). Typical discharge parameters were 2.6 Pa, 0.2 A, and 400 V. The thickness of the film was monitored by a quartz oscillator. The coating was continued until the thickness reached 200 nm (typically 72 min). In most cases, the coating was carried out at around room temperature. The temperature increased during the discharge because of power flow from the plasma, but was kept lower than 70°C. After the coating, the boron film was once heated up to 500°C to evacuate H atoms retained in the film during the coating.

In the stage (2), hydrogen and/or helium discharges were carried out to obtain hydrogen absorption and desorption characteristics. Typical discharge parameters were 2.6 Pa, 0.2 A, and 400 V for hydrogen, and 2.6 Pa, 0.2 A, and 250 V for helium.

In the stage (3), the liner was heated again up to 500°C to measure the desorbed number of H atoms from the film, and to reset the boron film into the starting condition of the stage (2).

After the B-coating and the heating (stage (1)), the stage (2) and the stage (3) were repeated alternately with various schemes of the discharge sequence in the stage (2). The hydrogen discharge, hydrogen discharge + helium discharge, and their repetition were mainly carried out. The procedure in stage (3) was identical through the all series of the experiment.

This procedure allowed us to obtain good reproducibility within ±2.5% because the condition of the boron film was once reset by the evacuation of hydrogen atoms with the stage (3). In Section 3, the experimental results of stage (2) and (3) are mainly presented. Renewing coatings were occasionally carried out several times. The boron films which had almost same characteristics were produced.

Depth profile of H atoms in the film was measured by elastic recoil detection method (ERD) [19]. A substrate of 10 × 20 mm made of SS was placed on a sample holder and set under the same condition as the liner surface (see Fig. 1). It was coated together with the liner. After the coating and/or exposure to the plasma, the substrate was taken out and set in another chamber for the ERD. Helium ions of 1.5 MeV were generated by AN-2000 Van de Graaff accelerator in Nagoya University and bombarded on the sample at an incident angle of 10° from the sample surface. A solid state detector for ERD was placed at scattered angle of 20°, with a slit and a myler filter of 6 μm thick to cut the scattered He ions. A detector for rutherford back scattering (RBS) is also set at 150° from the beam to monitor He ion fluence and film thickness [19,20].

Detailed description of the device is given in Ref. [21].

3. Experimental results

3.1. Hydrogen glow discharge

Fig. 2 shows a typical time evolution of the total pressure measured by a DG during a glow discharge in hydrogen. No change was observed in any gas species other than hydrogen with the QMS measurements. Thus, the total pressure is regarded as the hydrogen pressure. The flow rate and the pumping speed were kept constant at 26 ccm and 15.4 l/s, respectively. Before the ignition of the discharge, the pressure was constant at 2.6 Pa. The pressure decreased with a time constant of 8 s just after the ignition. It corresponds to the pumping characteristic time of this device.

The pressure slowly increased when the discharge was continued. When the discharge was turned off, the pressure once increased and then decreased to a constant value as shown in Fig. 3, which shows the total pressure at around turning off of the discharge for the same data as Fig. 2. This transient increase is regarded as a release of over saturated hydrogen atoms in the film during the discharge. Similar behavior has been reported in Tokamaks and Heliotron E [17,22], and it has been found for the first time for boron films under a glow discharge condition.

The constant value after the discharge agrees with that before the discharge within ±0.4%, which corresponds to an error bar in Fig. 3. The pressure difference between before and after the termination of the discharge is larger than the error bar. It means that hydrogen atoms are continuously absorbed until the end of the 1 h discharge. Such a phenomenon has been reported for ion beam irradiation to some kinds of carbon pieces [23], and found for the first time for a boron film under the plasma irradiation. This effect is discussed again in Section 3.4 with results of thermal desorption.

Total amount of absorbed H atoms was calculated by integrating pressure drop from the baseline in Fig. 2 multiplied by pumping speed. The value obtained in the case of Fig. 2 was $(9.2 \pm 0.4) \times 10^{16}$ H atoms/cm^2, which is the same order of magnitude as the saturation value in other measurements [24–28].

When the graphite liner was used, basic behavior was the same. The absorbed amount was, however, two times higher with graphite liner than with stainless steel

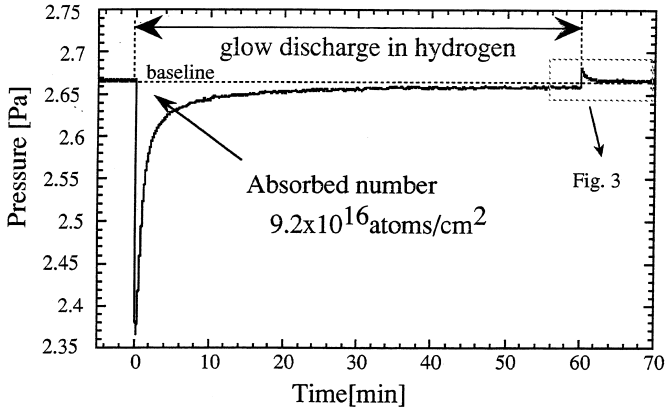

Fig. 2. Time evolution of total pressure during glow discharge in hydrogen. The discharge current and voltage are 0.2 A and 400 V, respectively. The pumping speed (15.4l/s) and hydrogen flow rate (26.0 ccm) are kept constant. The pressure decreased due to hydrogen absorption into the boron film.

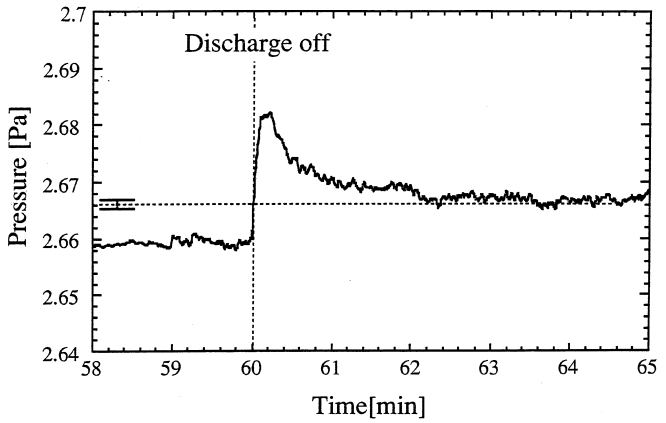

Fig. 3. Total pressure around turning off of the discharge for same data as Fig. 2. The pressure once increased and then decreased to the constant value, which is larger than the pressure during the discharge.

liner. The other behavior was almost the same except for the absolute value.

3.2. Helium glow discharge

To measure the behavior of hydrogen desorption by helium ion bombardment, a glow discharge in helium was carried out after the hydrogen discharge of 1 h. Fig. 4 shows time evolution of the hydrogen pressure measured by QMS. The QMS signal is converted to absolute partial pressure by a calibration with the diaphragm gauge. The pressure rapidly increased with the same time constant as the pumping system. It means that hydrogen atoms are immediately desorbed by the He ion impact. The pressure decreased during the discharge and became the background level within 15 min. Total amount of desorbed hydrogen atoms was calculated by the similar procedure as in the case of hydrogen discharge, and estimated to be $(1.3 \pm 0.4) \times 10^{16}$ H atoms/cm^2. It corresponds to 15% of the absorbed hydrogen during 1 h H_2 discharge.

To measure a recovery of hydrogen absorption capability of the boron film, a hydrogen discharge was carried out after the helium glow discharge as schematically shown in the upper part of Fig. 5. The rapid and strong absorption was observed again in the initial phase of the discharge. The absolute value of the pressure change is indicated in the figure to compare the absorbed and desorbed number clearly. Total amount of H absorbed during the second H_2 discharge is larger than the one desorbed during the He discharge. This effect is another new finding of this study, and discussed again in Section 3.4 with the results of thermal desorption experiments.

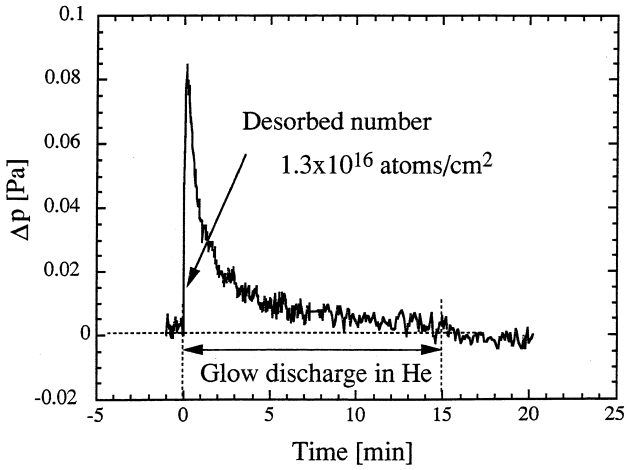

Fig. 4. Time evolution of hydrogen partial pressure measured by QMS. The discharge current and voltage are 0.2 A and 500 V, respectively.

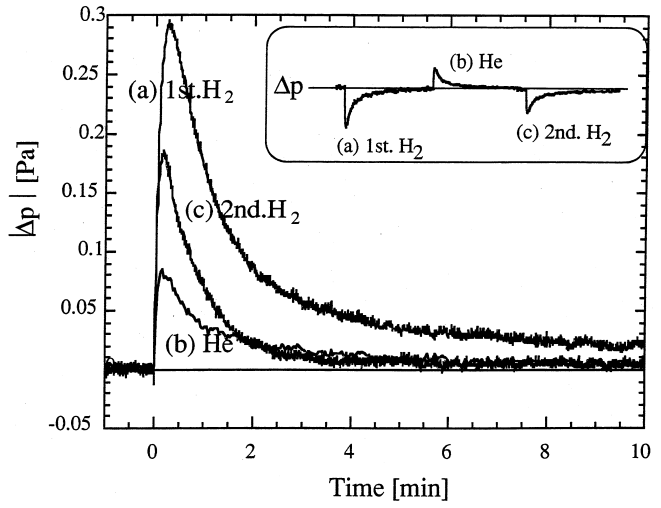

Fig. 5. Absolute value of pressure change during H_2/He discharges. The procedure is schematically shown in upper part of this figure.

3.3. Thermal desorption

To measure thermal desorption characteristics, the whole liner was heated up to 500°C. Fig. 6 shows time evolution of the H_2 pressure and the liner temperature, during the heating after the 1 h H_2 discharge. The hydrogen pressure was measured by QMS calibrated with the diaphragm gauge.

The liner temperature increased at a rate around 10°C/min. The H_2 pressure increased almost linearly until a peak value around 400°C. The pressure decreased when the liner temperature was increased to and kept at 500°C for 30 min. The pressure is plotted as a function of the liner temperature in Fig. 7 for the same data as Fig. 6. The peak is seen more clearly at 380°C. Similar behavior has been reported in Refs. [29,30] for small test species. It has been demonstrated for relatively large surface area of 7000 cm^2.

Total amount of H atoms desorbed was calculated by integrating the curve in Fig. 6 and estimated to be $(11 \pm 0.05) \times 10^{16}$ H atoms/cm^2. This is slightly larger than but close to the amount of H atoms absorbed during the H_2 discharge (see Section 3.1).

The accuracy in estimation of the total amount of hydrogen atoms is higher in the thermal desorption measurement (±0.5%) than in the H_2 discharge (±4%) or the He discharge (±30%) mainly because the drift of the baseline in the thermal desorption is small compared to the signal intensity. Detailed discussion about the accuracy is given in Ref. [21].

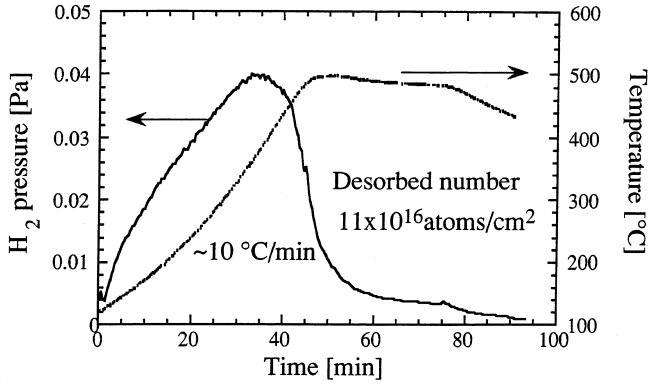

Fig. 6. Time evolution of hydrogen pressure and liner temperature during thermal desorption.

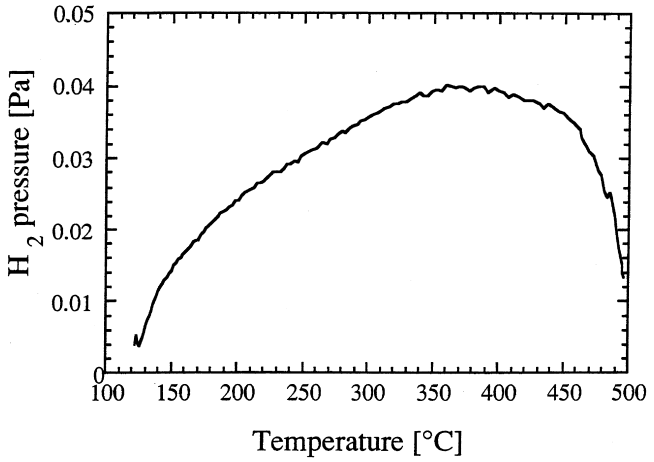

Fig. 7. Hydrogen pressure against liner temperature obtained from data of Fig. 6.

3.4. Discharge experiments and thermal desorption

To confirm slow and continuous absorption of H atoms after the near saturation at 30 min, a hydrogen discharge for 3 h was carried out. The result is shown in Fig. 8, where vertical axis shows the relative change in retained number of H atoms, which was estimated by integration of the pressure change. The number increased continuously up to 3 h and became 1.3 times higher than that at 1 h. Even when the discharge continued up to 10 h, the absorption continued without saturation.

The dotted lines in the figure show time evolution of H retained during thermal desorption after H_2 discharge for 1 h and 3 h, respectively. The retained number decreased and returned to the initial value in each case. It means that most of absorbed H atoms can be desorbed by heating.

To confirm H accumulation/desorption by H_2/He discharges, glow discharge in H_2 and He (each 15 min) were repeated 4 times after the H_2 discharge of 1 h. Similarly to Fig. 8, the relative change in retained number of H atoms is shown in Fig. 9. The number of H atoms decreased during He discharges due to the ion impact desorption. The number increased rapidly at the initial phase during H_2 discharge. After the rapid absorption, the hydrogen absorption continued slowly without saturation until stop of the discharge. The retained number increased gradually by the repetition of the discharges. The results of thermal desorption experiments are also shown in the figure, which shows that most of the accumulated H atoms can be desorbed by the heating in this case, too.

From these results and the shape of the curve in Fig. 6 which has the peak value, we can conclude that hydrogen atoms implanted during the discharges were evacuated by the heating up to 500°C. The required temperature for the H evacuation is regarded as 400°C from the peak position. This temperature is much lower than that for carbon wall of 900°C [31] and B/C coating of 700°C [4,32]. This is important for application to a

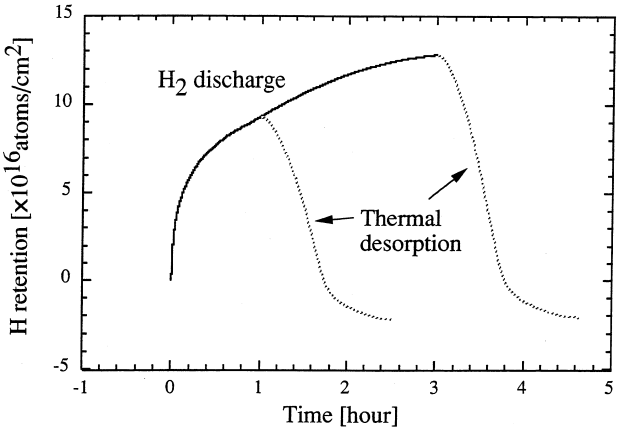

Fig. 8. Hydrogen accumulation during long term H_2 discharge. Dotted lines show decrease of hydrogen atoms during thermal desorption.

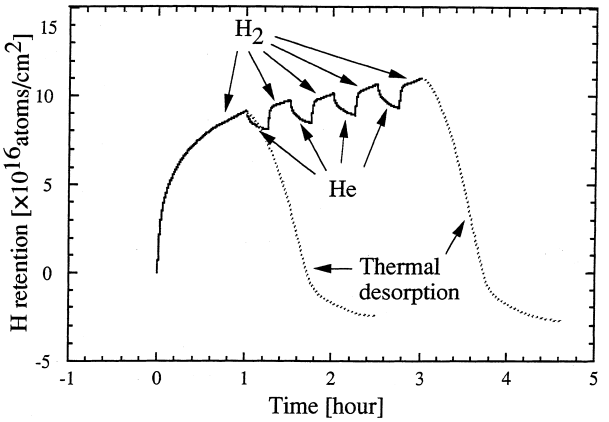

Fig. 9. Time evolution of retained number of H atoms when H_2 and He discharges are repeated alternately. The data during thermal desorption are also shown.

fusion device and discussed later in Section 4.2. In every thermal desorption, the desorbed number was slightly larger than the absorbed one in the preceded hydrogen discharges. The possible explanation is given as follows. Some of the H atoms deposited during the coating cannot be desorbed by the heating up to 500°C. They are slowly moved to the surface from the deeper layer during cooling from the elevated temperature. Part of them are desorbed during the next heating, and thus, the desorbed number was slightly larger than the absorbed.

3.5. Depth profile measurements

The depth profile of the H atoms was measured using the ERD method. Fig. 10 shows depth profile obtained in cases of (a) after the B-coating and subsequent thermal desorption, (b) 1 h exposure and (c) 3 h exposure to the H_2 glow, respectively.

After thermal desorption (case (a)), the hydrogen density was low and uniformly distributed over the whole depth up to 110 nm, which was the same as the film thickness measured by RBS method. It means that hydrogen atoms were retained only in the boron film and not in the stainless steel substrate. The thickness by RBS was roughly a half of that measured by quartz oscillator thickness monitor. It is probably because the location of the thickness monitor is slightly inside the liner. The H density was about 1/8 of that in the as-coated sample. The H atoms were retained during the deposition of the film and were not removed out by the heating at lower temperature than 500°C probably because of their larger binding energy. It is consistent with the fact that the desorbed number in the thermal desorption experiments is slightly larger than the absorbed one.

In cases of (b) and (c), the density of only near surface region (~70 nm) increased. When the discharge

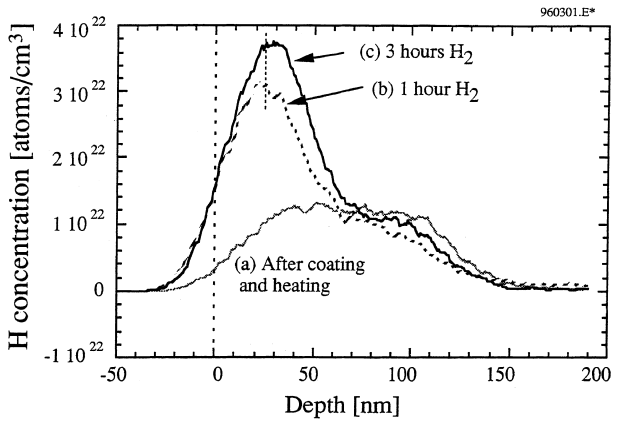

Fig. 10. Depth profile of H atoms measured by ERD.

continued to 3 h, the peak density increased and the peak position slightly shifted to deeper level compared to the case of the 1 h exposure.

The resolution of the ERD measurements is around 15 nm [33]. The real profile of hydrogen is sharper if the resolution is taken into account. Relation between the detected depth profile $N_{\mathrm{DET}}(x)$ and the real profile $N_{\mathrm{REAL}}(x)$ is described as follows with use of Gaussian distribution for the detector resolution as follows:

$$N_{\mathrm{DET}}(x) = \int N_{\mathrm{REAL}}(t-x)\, g(t)\, \mathrm{d}t,$$

where

$$g(t) = \frac{1}{\sigma\sqrt{\pi}} \exp\left(-\frac{t^2}{\sigma^2}\right):$$

Gaussian distribution function

σ: resolution

x: depth

For simplicity, we assumed real density profiles of square type with non-zero background level as indicated hatched area in Fig. 11. The background level was determined from the case (a) in Fig. 10 since it is uniform. The profile (A) and resolution σ were determined to obtain best fit to the profile of 1 h (case (b) in Fig. 10). The saturation level was estimated to be 1.0×10^{22} atoms/cm^3, which is the same order as the density of boron atoms. It should be noted that the concentration of the background level is much lower than the saturation level in the real profile, though they seem comparable in detected profile in Fig. 10.

We gave two kinds of square type distribution to $N_{\mathrm{REAL}}(x)$ for the case of 3 h exposure; (B) higher density (open squares) and (C) broader depth (close squares). An increment in the height and the depth was taken as 30% from the increasing rate of retained H shown in thermal desorption experiments. The calculated profiles are indicated in Fig. 11. In spite of small difference between (B) and (C), the peak clearly shifted to the deeper

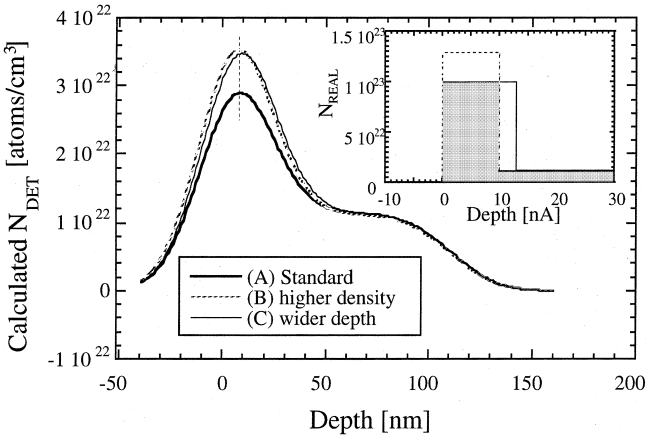

Fig. 11. Calculation of detected profile from model profile. Model profile of square type is assumed. The experimental results are reproduced.

side in (C) compared to (B) and (A). In addition the assumption (C) seems more reasonable if we assume the saturation density.

Thus, it is concluded that hydrogen atoms are retained only in the near surface region of ~10 nm, which is the same order of magnitude as its implantation range and much smaller than the film thickness of 110 nm. The increase in H retention during long term discharge can be explained by deeper migration of the hydrogen atoms into the film, but the migration is limited in the near surface region. These findings are important for application and discussed again in Section 4.2.

4. Discussion

4.1. Modeling of hydrogen behavior

Several models to describe hydrogen behavior in graphite and amorphous carbon have been reported [31,33–36]. Most of the models assume the existence of trapped and solute (mobile) hydrogen atoms, and the effects of de-trapping, trapping, diffusion, and desorption are considered. The trapping state of H atoms in boron film is not well understood. However, it is confirmed experimentally that, at around room temperature, the hydrogen atoms remaining at the trapping sites after the implantation do not move at least for a few days. It means that hydrogen atoms are trapped in the boron film similarly to the H atoms in carbon. A simple model is developed based on the conventional models for graphite and amorphous carbon, and the calculated results are shown in this section.

The transient behavior just after turning on and off of the discharge has been investigated. Here, the slow migration of the H atoms can be neglected. In addition, following conditions are assumed; (a) thermal detrapping can be neglected at around room temperature, (b) ion implantation is uniform in depth within its implantation range, and (c) ion impact detrapping is also uniform.

The differential equation during the hydrogen discharge can be written as follows:

$$\frac{\partial c_s}{\partial t} = S_r - 2k_{ss}c_s^2 - k'_{ss}c_s c_t - k_{st}c_s(c_T - c_t) + \sigma_d \Phi_i c_t, \quad (1)$$

$$\frac{\partial c_t}{\partial t} = k_{st}c_s(c_T - c_t) - \sigma_d \Phi_i c_t - k_{ss}c_s c_t, \quad (2)$$

where c_s and c_t are the hydrogen density of 'solute' and 'trapped', respectively. Here, the local recombination is assumed as in models for graphite and amorphous carbon. Two kinds of recombination process, namely 'solute – solute' and 'trapped – solute', are possible. They correspond to second and third term of the right-hand side of Eq. (1), respectively. c_T is the density of the trap site, k_{st} the trapping rate coefficient, and σ_d the ion impact de-trapping cross-section. S_r denotes the source term due to hydrogen implantation. S_r is estimated from the experimental value of the maximum absorption flux on assumption that all of the injected hydrogen atoms are absorbed at initial phase. The ion flux Φ_i is estimated from the discharge current.

First, the transient release of the H atoms after the termination of the H_2 discharge was modeled. Before the termination, the incident flux and re-emission flux are balanced. The incident flux rapidly decreased after the termination of the discharge, which could result in strong net desorption of H atoms. However, the desorption flux is an order of magnitude lower than the incident flux. This behavior can be understood if we assume that time constant of trapping are much shorter than that of the re-emission. In such case, most of the hydrogen atoms are immediately trapped after the termination of the discharge except for over saturated H atoms due to H implantation during the discharge, and the hydrogen release is attributed to recombination of the over-saturated H atoms. Then the differential equation (1) and (2) reduce to

$$\frac{\partial c_s}{\partial t} = -2k_{ss}c_s^2 - k'_{ss}c_s c_t. \quad (3)$$

Time evolution of H re-emission is calculated based on the Eq. (3) for two extreme cases, that is, the recombination occurs only through the processes of (i) 'solute – solute' or (ii) 'trapped – solute'. Both can be solved analytically and the results for assumption (i) and (ii) are

$$\Phi = \frac{R_i}{2k_{ss}} \frac{1}{(t + 1/2k_{ss}c_0)^2}, \quad (4)$$

$$\Phi' = c_0 R_i k'_{ss} c_t \exp(-k'_{ss}c_t t), \quad (5)$$

where Φ is the H re-emission flux from the film, R_i is the implantation range and c_0 is the initial concentration of over saturated H atoms. The $c_0 R_i$ corresponds to total amount of over saturated H atoms and estimated to be 1×10^{15} H atoms/cm^2 by integrating the curve in Fig. 3.

The results are shown in Fig. 12(a) and (b) for the assumption (i) and (ii), respectively. The experimental data are calculated from the pressure change in Fig. 3 by using the mass balance equation as follows:

$$V\frac{dp}{dt} = Q - S_p p + \beta A \Phi, \quad (6)$$

where V is the volume of the chamber, Q the source rate due to external gas injection, p the pressure, S_p the pumping speed, A the surface area of the liner, and β a conversion factor. The solid line in the figure shows results of the calculation. In Fig. 12(a), the calculated results agree well with the experimental results. On the other hand, the calculation does not give agreement with the experimental results in Fig. 12(b). It is concluded that

the recombination of two solute H atoms is dominant. The product of $k_{ss}R_i$ is estimated from the best fitting value. The R_i is estimated to be 6.5 nm based on TRIM code calculation for 200 eV H implantation (and thus, 400 eV H_2) [37]. Then, the k_{ss} is estimated as 7.8×10^{-24} cm^3/s.

When it is assumed that a quasi-steady state attains in later phase of the hydrogen discharge, the Eqs. (1) and (2) reduce to

$$S_r = 2k_{ss}c_s^2, \tag{7}$$

$$k_{st}c_s(c_T - c_t) = \sigma_d \Phi_i c_t. \tag{8}$$

Substituting the values estimated above into Eq. (7), c_s is estimated to be 8.8×10^{21} H atoms/cm^3. If we assume the c_T to be 4×10^{22} H atoms/cm^3, which corresponds to $H/B = 0.4$, the c_t in quasi-steady state is estimated to be 3.2×10^{22} H atoms/cm^3 from the following equation:

$$c_t + c_s = c_T + c_0, \tag{9}$$

where c_0 is the concentration of over saturated H atoms. It is estimated to be 1.5×10^{21} H atoms/cm^3 from the integration of the curve in Fig. 3 and R_i obtained by TRIM calculation.

Substituting these values to Eq. (8), the ratio

$$k_{st}/\sigma_d = 0.21 \text{ [cm/s]} \tag{10}$$

is obtained. Both σ_d and k_{st} are considered to be constant during the discharge in Eqs. (1) and (2), and thus, the ratio is constant. The k_{st}/σ_d ratio depends on the assumption of the density of the trap site. The following

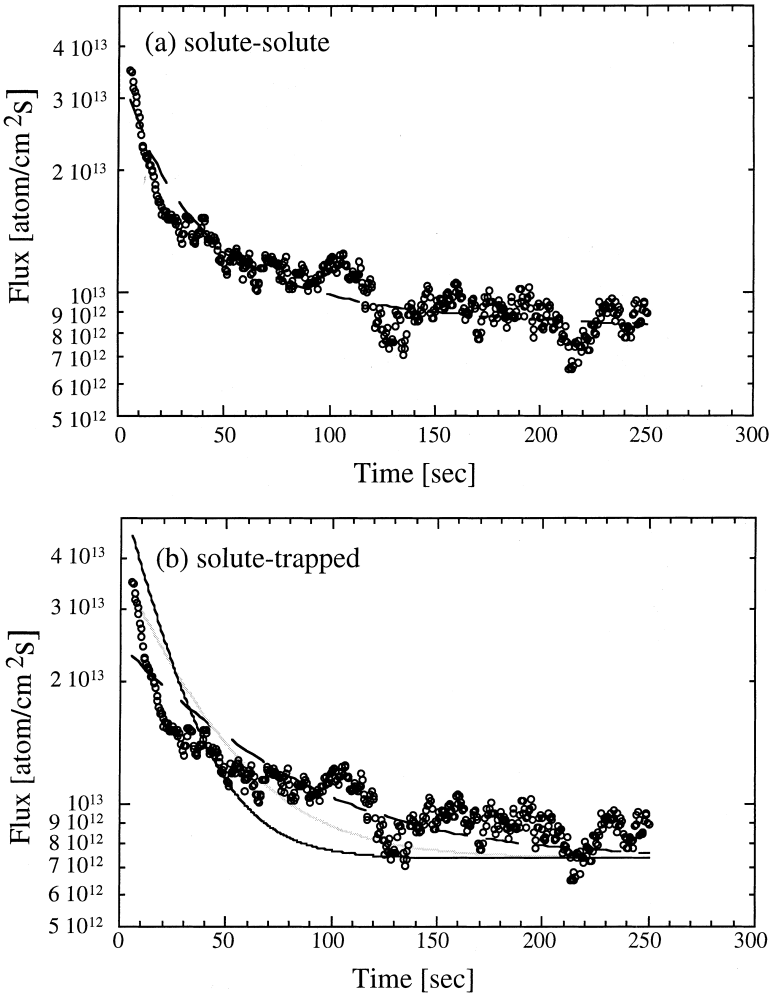

Fig. 12. Hydrogen desorption flux after termination of hydrogen discharge. The open circles show experimental results. The lines show calculated results for two extreme cases: (a) recombination of two solute H atoms is dominant, (b) recombination of solute and trapped H atoms is dominant. The assumption (a) agrees better with the experimental results.

results are, however, not strongly affected by the assumption.

The time evolution of the solute and trapped hydrogen density after the termination of the H_2 discharge was calculated again based on Eqs. (1) and (2), by using the steady state densities estimated above as the initial densities just before the termination of the discharge. The calculation was carried out for wide range of the σ_d and k_{st}. The ratio k_{st}/σ_d was kept constant under the condition of Eq. (10). The hydrogen re-emission flux Φ is estimated from the relation $\Phi = 2k_{ss}c_s^2 \cdot R_i$. The results are shown in Fig. 13. Similarly to Fig. 12, the experimental flux was estimated from the pressure change in Fig. 3. The strong desorption is observed which is higher by an order of magnitude than the experimental results, when the detrapping cross-section is smaller than 10^{-23} cm^2, as shown by a curve (b). The strong re-emission rapidly decreased within a second when the de-trapping cross-section are larger than 10^{-20} cm^2, as a curve (a). It is interpreted that the hydrogen atoms in the solute state under the ion bombardment are immediately trapped and the over saturated H atoms are released with a time constant of ~1 min as is assumed in the above calculation for the recombination. Under this experimental condition, the rapid re-emission could not be observed because the time constant of the re-emission is much smaller than that of the pumping system of 8 s. Thus it is concluded that the calculated results agree with the experimental result.

The hydrogen behavior during helium discharge was calculated with similar procedure. The source term S_r was eliminated. The initial condition was set as $c_s = 0$ and $c_t = c_T$. First, the same ratio as Eq. (10) was used. The calculation was carried out for wide range of the cross-section. The calculation resulted in typical three cases, namely, the detrapping cross-section is (a) large enough ($>10^{-20}$ cm^2), (b) small enough ($<10^{-23}$ cm^2), and (c) intermediate ($\sim 10^{-22}$ cm^2). The use of larger value than (a) or smaller value than (b) did not change each curve. Fig. 14 shows the hydrogen desorption behavior for the three cases. In cases (b) and (c), the sharp desorption after the ignition is not observed. The time behavior in case (a) is similar to the experimental results, except for difference in the absolute value. The difference can be attributed to the ion induced detrapping cross-section. Consequently, it results in the change in the ratio of k_{st}/σ_d. Fig. 15 shows the best fitting of the calculated data together with the experimental results. It was found that if we assume the detrapping cross-section of five times lower than that for hydrogen ion impact, the experimental results can be well reproduced.

From these considerations, it has been found that hydrogen desorption during the He discharge and hydrogen release after the termination of the hydrogen discharge can be described when the hydrogen trapping rate coefficient and the de-trapping cross-section are sufficiently large. The intermediate value of $\sigma_d \sim 10^{-22}$ cm^2 corresponds to the condition in which the de-trapping rates (Eq. (8)) are comparable to the desorption rates (Eq. (7)) at the typical density. When the trapping rate coefficient and then, the de-trapping cross-section are large enough, the hydrogen atoms in solute state are maintained by a balance between trapping and detrapping under ion bombardment. The slow absorption effects may be driven by the migration of these solute atoms deeply into the film.

The time evolution of the absorption flux at initial phase of the H_2 discharge was calculated for the case

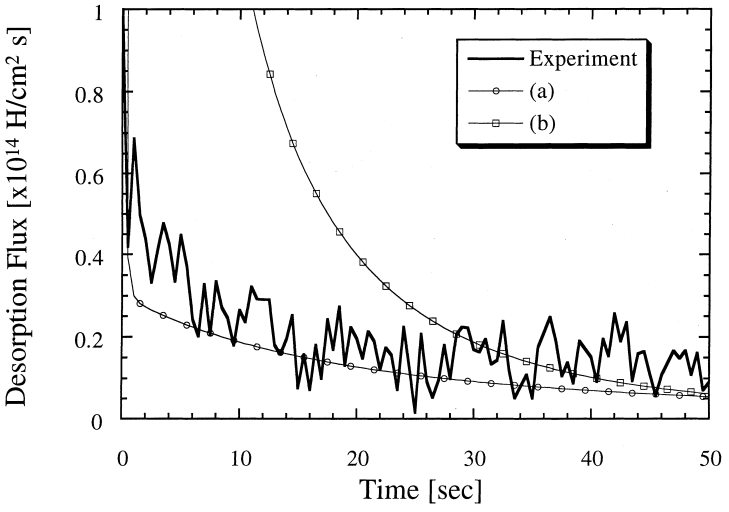

Fig. 13. Time evolution of hydrogen desorption flux after termination of discharge. Calculated results are shown for the cases of (a) $\sigma_d = 10^{-23}$ cm^2, and (b) $\sigma_d = 10^{-20}$ cm^2.

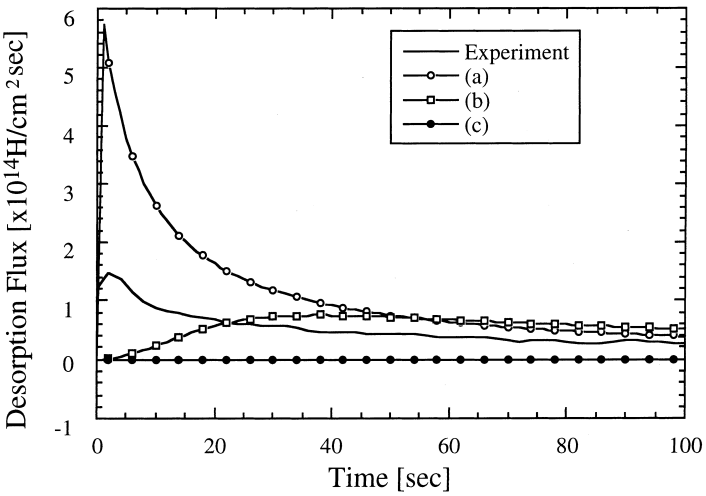

Fig. 14. Hydrogen desorption flux at initial phase of He discharge. Calculated results are shown for three cases; trapping rate coefficient and detrapping cross-section are: (a) large enough ($\sigma_d = 10^{-20}$ cm^2), (b) intermediate ($\sigma_d = 10^{-23}$ cm^2), and (c) small enough ($\sigma_d = 10^{-25}$ cm^2).

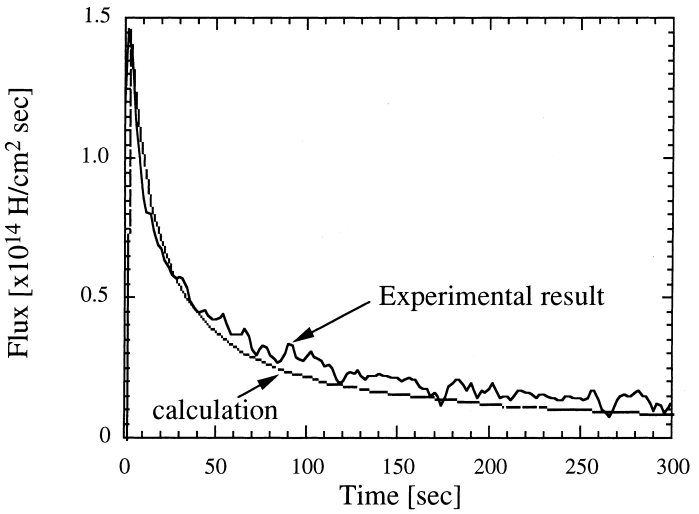

Fig. 15. Hydrogen desorption flux during He discharge. The calculated results agree well with the experimental results if the ion induced detrapping cross-section of five times smaller than that of hydrogen ion impact.

of large trapping and detrapping (10^{-20} cm^2). Fig. 16 shows the calculated results together with the experimental results (solid thick line). In the experimental result, the strong net absorption at initial phase of the discharge rapidly decreased. On the other hand, the strong absorption continued for a few tens of seconds in calculated result. The calculated result does not agree with the experimental results. The reason for this difference is not well understood. A possible explanation for this difference is that the atomic hydrogen atoms, which do not penetrate into the film, accumulate on the surface and re-emitted from the initial phase. To understand this behavior quantitatively, the depth profile of hydrogen implantation must be considered.

4.2. Application for protection wall against tritium permeation

Through this study, it has been demonstrated that (1) hydrogen atoms are retained only in the near surface region around their implantation range, and (2) most of the implanted hydrogen atoms can be desorbed by the

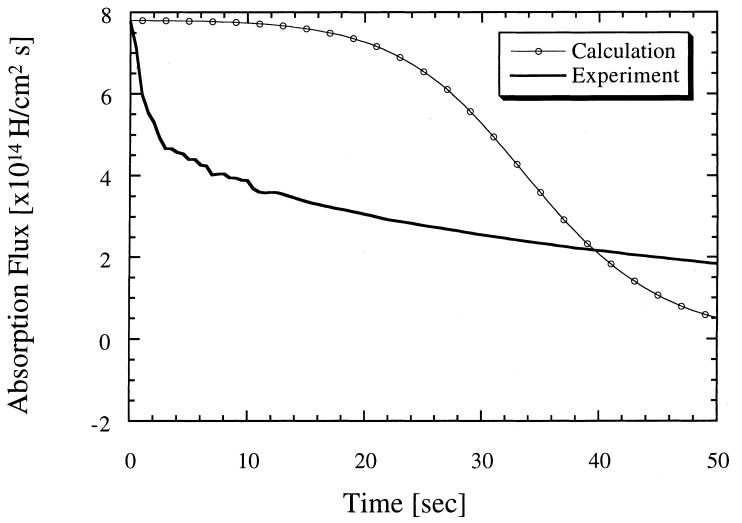

Fig. 16. Hydrogen absorption at initial phase of H_2 discharge. Calculated results are shown for the case of large detrapping cross-section ($\sigma_d = 10^{-20}$ cm^2).

heating up to 400°C. These favorable characteristics gives an idea of a protection wall against tritium permeation [19].

In future fusion devices, the first wall is exposed to charge exchange neutral tritium atoms, which have relatively high energy. It will induce considerable tritium inventory and its permeation to cooling channels. However if the wall is coated by a boron film, implanted tritium atoms remain only in the near surface and are desorbed from the film toward the plasma side. It is possible to keep the temperature of the first wall high with use of heat load from the plasma. In this case, the first wall design becomes easier with boron coating because the required temperature for the tritium evacuation is much lower than that for carbon wall, and thus, the temperature difference between the first wall and the coolant becomes smaller.

The present experiment has shown up these very promising characteristics of boron films. It is necessary to confirm this possibility further by additional experiments such as an actual investigation on permeation etc.

5. Conclusion

It has been found that there are two components in hydrogen absorption into the boron film at around room temperature. One is strong and short absorption to the H depleted near surface. The other is the slow and long lasting absorption.

Around 15% of injected H atoms were desorbed by helium ion impact. The helium ion may cause migration of hydrogen atoms deeply into the film, and thus, the hydrogen atoms are accumulated in the film when the H_2 and He discharges are repeated alternately.

The hydrogen atoms are retained only in the near surface region which is the same order as its implantation range and much smaller than the film thickness of 110 nm. Most of them can be released by the heating up to 400°C, even when the boron film is exposed to the hydrogen discharge for a long term. These are favorable characteristics for applying B-films as a protection wall against tritium permeation.

A simple model to describe hydrogen behavior has been proposed. It has been found that the recombination between two solute hydrogen atoms are dominant in the re-emission process, and the recombination coefficient is estimated to be 7.8×10^{-24} cm^3/s from the analysis for transient hydrogen release just after the termination of the hydrogen discharge.

Transient behavior after the ignition of H_2 and He discharge has been modeled based on the findings about the recombination. The calculated results with this model agree fairly well with the experimental results. It has been found through the calculation that the hydrogen atoms around 20% of the saturation density are in solute state, which is maintained by a balance between trapping and detrapping. The slow absorption may be caused by the migration of the detrapped H atoms deeply into the film. The depth profile measured by ERD gives consistent results with this consideration.

References

[1] J. Winter, J. Nucl. Mater. 145–147 (1987) 131.
[2] J.P. Coad, K.H. Behringer, K.J. Dietz, J. Nucl. Mater. 145–147 (1987) 747.
[3] N. Noda et al., Jpn. J. Appl. Phys. 25 (1986) L397.
[4] J. Winter et al., J. Nucl. Mater. 162–164 (1989) 713.

[5] G.L. Jackson et al., J. Nucl. Mater. 196–198 (1992) 236.
[6] M. Saidoh et al., Fusion Eng. Design 22 (1993) 271.
[7] U. Schneider et al., J. Nucl. Mater. 176&177 (1990) 350.
[8] H.F. Dylla et al., J. Nucl. Mater. 176&177 (1990) 337.
[9] H. Yamada et al., Jpn. J. Appl. Phys. 33 (1994) L1638.
[10] P.R. Thomas, J. Nucl. Mater. 176&177 (1990) 3.
[11] J.D. Strachan et al., J. Nucl. Mater. 217 (1994) 145.
[12] N. Noda, J. Nucl. Mater. 220–222 (1995) 623.
[13] J. Ehrenberg, J. Nucl. Mater. 162–164 (1989) 63.
[14] S. Higashijima et al., J. Nucl. Mater. 220–222 (1995) 375.
[15] N. Noda, In Contribution to High-temperature Plasma Physics, Akademie Verlarg, Berlin, 1994, p. 21.
[16] D.S. Walsh, B.L. Doyle, W.R. Wampler, A.K. Hays, J. Vac. Sci. Technol. A 9 (1991) 727.
[17] N. Noda et al., J. Nucl. Mater. 162–164 (1989) 769.
[18] J. Ehrenberg et al., J. Nucl. Mater. 196–198 (1992) 992.
[19] K. Tsuzuki et al., J. Nucl. Mater, in press.
[20] M. Natsir et al, Vacuum 47 (1996), in press.
[21] A. Sagara et al., Rev. Sci. Instrum., to be published.
[22] P. Andrew, M. Pick, J. Nucl. Mater. 220–222 (1995) 601.
[23] A.A. Haasz, J.W. Davis, J. Nucl. Mater. 209 (1994) 155.
[24] M. Yamage, T. Ejima, H. Toyoda, H. Sugai, J. Nucl. Mater. 196–198 (1992) 618.
[25] B.L. Doyle, W.R. Wampler, D.K. Brice, S.T. Picraux, J. Nucl. Mater. 93&94 (1980) 551.
[26] Y. Yamauchi et al., J. Nucl. Mater. 220–222 (1995) 851.
[27] J. Von Seggern et al., J. Nucl. Mater. 176&177 (1990) 357.
[28] D.S. Walsh et al., J. Vac. Sci. Technol. A 9 (1991) 727.
[29] H. Toyoda, T. Isozumi, H. Sugai, T. Okuda, J. Nucl. Mater. 162–164 (1989) 732.
[30] T. Hino et al., Thin Solid Films 253 (1944) 518.
[31] W. Moller, J. Nucl. Mater. 162–164 (1989) 138.
[32] R. Jimbou, M. Saido, N. Ogiwara, T. Ando, J. Nucl. Mater. 196–198 (1992) 958.
[33] K. Morita, K. Ohtsuka, Y. Hasebe, J. Nucl. Mater. 162–164 (1989) 990.
[34] B.L. Doyle, W.R. Wampler, D.K. Brice, S.T. Picraux, J. Nucl. Mater. 93&94 (1980) 551.
[35] S. Yoshida, H. Sugai, H. Toyoda, Jpn. J. Appl. Phys. 28 (1988) 1101.
[36] A.A. Haasz, P. Franzen, J.W. Davis, S. Chiu, C.S. Pitcher, J. Appl. Phys. 77 (1995) 66.
[37] J.P. Biersack, W. Eckstein, Appl. Phys. A 34 (1984) 73.